

Experimental and Numerical Study on the Influence of Liner Height on Explosively Formed Projectiles

V. Minh Do¹, D. Thanh Tran¹, H. Quan Pham^{1*}, X. Son Bui¹,
H. Nguyen Pham² and D. Tho To³

¹ Faculty of Weapons, Le Quy Don Technical University, Hanoi, Vietnam

² Faculty of Military Technology, Tran Dai Nghia University, HoChiMinh, Vietnam

³ Division of Military Science Technical and Technology, Military Science Department, Vietnam

The manuscript was received on 31 January 2025 and was accepted after revision for publication as an original research paper on 11 May 2025.

Abstract:

Explosively Formed Projectiles (EFP) are widely used in both military and civilian sectors for their ability to strike distant targets effectively. This study investigates EFP formation and penetration using Ansys Autodyn simulations and experimental validation. Focusing on the EFP warhead structure, it analyzes how liner height influences projectile performance. Results show that variations in liner height significantly affect the EFP's velocity, penetration depth, and diameter in steel targets. The study finds that an optimal liner height between 0.2 and 0.3 times the liner diameter yields the best projectile shape and dynamics. These findings offer practical guidance for selecting liner geometry in EFP warhead design.

Keywords:

explosively formed projectile, liner height, penetration, Ansys Autodyn

1 Introduction

Explosively formed projectile (EFP) is a specialized type of energy-concentrating explosive commonly used in munitions to destroy armored targets at long ranges. The typical structure of the explosively formed projectile warhead (EFPW) includes a casing, explosive charge, liner, detonator, and additional components (Fig. 1). Upon detonation, the shock wave compresses the liner surface, forming the EFP. Due to the unique design and shape of the liner, the metal elements in the EFP maintain uniform velocity, minimizing deformation and preventing fragmentation, allowing the EFP to travel farther.

* Corresponding author: Faculty of Weapons, Le Quy Don Technical University, Hoang Quoc Viet 236, Hanoi, Vietnam. Phone: +84 862 48 64 18, E-mail: phquanstudying@lqdtu.edu.vn.

The penetration power of the EFP against armored targets can reach 0.3 to 1 time the warhead caliber [1, 2]. The design parameters of the liner, including the liner radius, outer radius, and center coordinates of the radius, allow for the creation of various liner configurations. Therefore, changing the EFP formation process can create different forward and reverse EFP, which in turn influence the penetration power and effective target range of the warhead. Numerous researchers have studied the impact of liner configurations on EFP formation and penetration ability against steel targets. Cardoso recommended reducing the liner thickness from 6 mm to 4 mm to enhance projectile velocity and penetration power [3]. Wu proposed a preliminary structure for liners in explosively formed projectile warheads [4]. Salkičević analyzed the effect of varying liner thickness, finding that liners with variable thickness (from top to edge) achieved higher EFP velocities compared to those with uniform thickness [5]. Jeremić et al. evaluated liner discrepancies between numerical simulations and analytical methods, reporting deviations of less than 13 % [6]. Couque and Hussain conducted experiments and recommended using Ansys Autodyn software with a modified Johnson-Cook (MJC) model for smaller error compared to Johnson-Cook (JC) model [7-9]. Yuan conducted numerical simulations and experimental studies on the EFP with polygonal shell to optimize the EFP with fins [10].

However, the effect of liner height on EFP formation and penetration behavior into steel targets has not been fully explored. The objective of this paper is to study the EFP formation process, parameters, velocity gradients and interactions with steel targets with varying liner heights using Ansys Autodyn 2D software. Additionally, the experiments were conducted with the same warhead parameters as those used in the numerical simulation method. Experimental results are analyzed and compared with simulation results.

2 Simulation Model and Material Model

2.1. Geometric Model and Calculation Method

The subject of this study is the 54 mm explosively formed projectile warhead in Fig. 1. The warhead consists of four main components: casing, explosive charge, detonator, and liner. The liner, made of CU-OFHC copper, has a hemispherical shape and is defined by its height h , diameter d , one outer radius r_1 , and inner radius r_2 . It also features a top thickness δ_1 , edge thickness δ_2 , and the distances from the center of the outer and inner radius on the OX axis of symmetry to the bottom of the warhead have lengths of X_1 , X_2 respectively. The casing is made of polyethylene plastic, designed in a cylindrical form with an outer diameter D , length L , wall thickness t_1 for the cylindrical part and bottom thickness t_2 . The C4 explosive charge is packed inside the casing, with the diameter d and the height l .

To determine the structural parameters for the study, in addition to the caliber (d), it is necessary to preliminarily select some input parameters. According to [3, 4], the liner thickness should vary from the top to the edge of the liner, and the charge length should range from 0.75 to 1.1 times the caliber. For this study, the liner thickness is set at 2 mm at the top and reduced to 1 mm at the edge. The charge length is 60 mm, and the casing thickness is 4.4 mm.

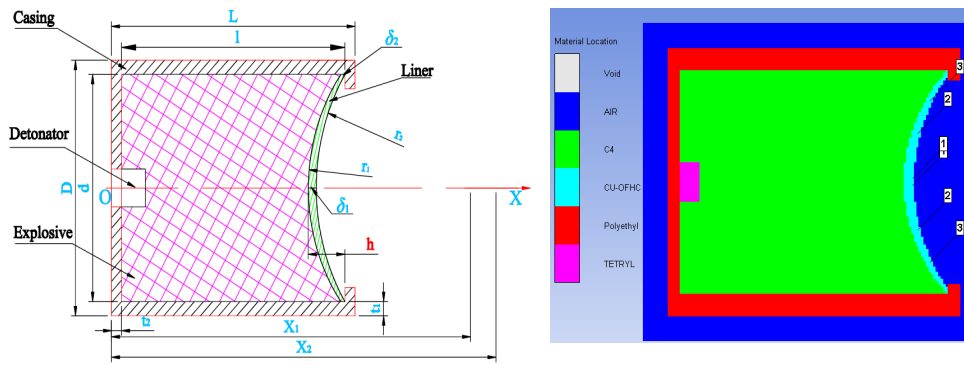


Fig. 1 EFPW model and simulation model in Autodyn

According to [1, 2], when the ratio $0.2 \leq h/d \leq 0.3$, the EFP achieves an optimal aerodynamic shape. Therefore, to study the influence of the liner height on the EFP formation process and the penetration depth of the EFP when interacting with the steel plate, the study has conducted tests and evaluated the h/d ratio in a wider range from 0.15 to 0.35. The parameters for the structural options are presented in Tab. 1.

Tab. 1 Parameters of EFPW with different liner heights

Size	Unit	Structure				
		1	2	3	4	5
D	mm	54				
d	mm	45.2				
L	mm	60				
l	mm	54.24				
t_1	mm	2.5				
t_2	mm	4.4				
δ_1	mm	2				
δ_2	mm	1				
X_1	mm	97.79	84.25	76.14	70.55	66.32
X_2	mm	108.5	90.27	80.31	73.81	69.07
r_1	mm	47.07	35.79	29.94	26.61	24.64
r_2	mm	55.78	39.8	32.11	27.87	25.39
h	mm	6.78	9.04	11.30	13.56	15.82
h/d		0.15	0.20	0.25	0.30	0.35

The Ansys Autodyn software is used to simulate the formation of the EFP and its interaction with steel targets. The parameters obtained from the EFP formation

simulation served as input data for simulating EFP impact on steel plate targets. Due to the axial symmetry and to reduce the computation time, the problem model used is a 2D symmetric model. The casing, liner, explosive, and air were modeled with a Eulerian grid, using a cell size of 0.25 mm × 0.25 mm. Flow out boundary conditions were applied to all computational domain boundaries except for the symmetry axis. The geometric model setup, including element selection, mesh sizing, geometry creation, material assignment, and gauge placement was conducted in the Autodyne-2D environment [6, 9-12].

2.2. Material Model and Parameters

The plastic explosive C4 is modeled as an ideal elastoplastic material that follows the Mises yield criterion. Upon detonation, C4 transitions into a gaseous state and is described using the Jones-Wilkins-Lee (JWL) equation of state. In this model, the detonation product pressure p is a function of the relative volume V and the specific internal energy E .

$$p = A \left(1 - \frac{\omega}{R_1 V} \right) e^{-R_1 V} + B \left(1 - \frac{\omega}{R_2 V} \right) e^{-R_2 V} + \frac{\omega E}{V} \quad (1)$$

where ω , A , B , R_1 , R_2 are the experimental constants, with values in Tab. 2 [6-8].

Tab. 2 Values of the parameters in the JWL equation for the state of C4 explosive

Parameters	Unit	Value
ρ	kg/m ³	1 601
A	kPa	6.0977×10^8
B	kPa	1.2950×10^7
R_1	–	4.5
R_2	–	1.4
ω	–	0.25
D	m/s	8 193
E	kJ/m ³	9.000001×10^6

The casing of the warhead is made of polyethylene plastic. Under explosive loading, the material undergoes significant volumetric and shape deformation. Therefore, the shock equation of state is used to describe its behavior. Parameters are experimental constants, with values in Tab. 3.

The liner is usually made of red copper $M1$ described by the modified Johnson-Cook (MJC) elastic-plastic model [6-8].

$$\sigma = \left(A + B \varepsilon_p^n \right) \left[1 + C \ln \left(\frac{\dot{\varepsilon}}{\dot{\varepsilon}_0} \right) + D \left(\frac{\dot{\varepsilon}}{\dot{\varepsilon}_l} \right)^k \right] \left[1 - \left(\frac{T - T_{\text{ref}}}{T_{\text{melt}} - T_{\text{ref}}} \right)^m \right] \quad (2)$$

in which σ – the dynamic yield stress; A , B , C , D , n , m and k are the constants of the material determined experimentally; ε_p – the plastic strain; $\dot{\varepsilon}$ – the plastic strain rate; $\dot{\varepsilon}_0$ – the reference value for plastic strain rate; $\dot{\varepsilon}_l$ – the reference strain rate charac-

terizing the transition between thermally activated and viscous regime; T_{melt} – the melting temperature of the material. In this simulation, the liner is composed of CU-OFHC copper and modelled using a Modified Johnson-Cook (MJC) model. To prevent plastic instability in the high strain rate regime ($10^3 \div 10^6$) s^{-1} , the material's hardening constant was increased by 10 %, from 29.2 GPa to 32.1 GPa. The target material, Steel 1006, is represented using the standard Johnson-Cook (JC) model. The parameters are in Tab. 4.

Tab. 3 Values of the parameters in the Shock equation for the polyethylene plastic

Parameters	Unit	Value
ρ	kg/m^3	915
Γ	–	1.64
C_1	m/s	2901
S_1	–	1.481
C_2	m/s	0
S_2	–	0

Tab. 4 Parameter values in the elastic-plastic model

Parameters	Unit	Value	
		CU-OFHC	Steel 1006
Equation of state	–	Linear	Shock
Density	kg/m^3	8 960	7 830
Melting temperature	K	1 356	1 811
Strength model	–	JC	JC
Yield stress A	GPa	0.09	0.35
Hardening constant B	GPa	0.3212	0.275
Strain rate constant C	–	0.025	0.022
Hardening exponent n	–	0.31	0.36
Thermal softening exponent m	–	1.09	1

To describe the equation of state of air in mathematical simulation, we use the gamma form of equation of state:

$$p = \rho(\gamma - 1)E \quad (3)$$

where $\gamma = 1.4$; $\rho = 1.225 \text{ kg/m}^3$, $E = 2.5 \times 10^5 \text{ J/kg}$ [13].

During the penetration process, the Lagrangian mesh is applied to both the EFP and the target. The simulation results of the EFP formation process using the Euler method are used to determine the EFP parameters. The target material is a sheet steel described in the software as Steel 1006 with a width of 200 mm and a thickness of

30 mm. The equation of state for the target material is the shock equation of state, while its strength model and failure model are the Johnson-Cook model (Tab. 5).

Tab. 5 Values of Johnson-Cook failure model parameters [14]

D_1	D_2	D_3	D_4	D_5
0.05	4.22	-2.73	0.0018	0.55

The simulation model of the impact process between EFP and steel target is shown in Fig. 2. Both EFP and target parts are modeled using 0.25 mm rectangular elements.



Fig. 2 Simulation of EFP impact on steel plate

3 Simulation Model and Material Model

The numerical simulation results of the formation and penetration process of EFP were confirmed by experimental methods. The simulation and experimental results, including the velocity and structural shape of EFP, were compared. For the penetration process of EFP, the hole diameter and penetration depth after impacting on a 20 mm thick steel target were compared.

3.1 Explosively Formed Projectiles and Experimental Target

The liner with structure 2 was selected for validation with the simulation model whose shape and size are shown in Tab. 1. The material of the forming liner is M1 copper. The shell is made of Polyethylene plastic. The explosive of EFPW is C4 plastic explosive. The No. 8 electric detonator is used to detonate the EFPW. The material of the target is 45# steel. The size of the target plate is 20 mm thick, 500 mm wide and 500 mm long in Fig. 3.

3.2 Experimental Setup

The experimental model for measuring the velocity and penetration of EFP is shown in Fig. 4. The tested EFPW is fixed horizontally and a 45# steel plate with a total thickness of 20 mm is placed in the distance of 3 m from the EFPW. At a distance of 2 m from the EFPW, an electronic timer (instrument type: UTC-8) was used to measure the velocity of EFP along its path. After the EFP interacts with the target steel plate, the diameter and depth of the penetration hole on the target steel plate will be measured.



Fig. 3 EFPW and steel target

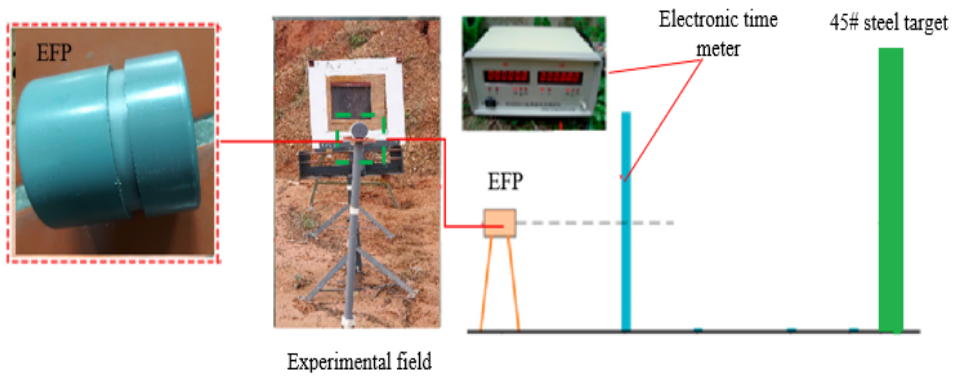


Fig. 4 Experimental measurement of EFP velocity and penetration depth

3.3 Experimental results

After the static blasting of the test specimens, the dimensions of the through hole on the steel plate were measured to determine its diameter and depth, as shown in Fig. 5.

The results of EFP velocity (V), hole width (W_h) and hole depth (D_h) when tested for each type of EFP with different liner curvature radius are shown in Tab. 6.

Tab. 6 EFP velocity and penetration results on steel target (structure 2)

Symbol	0.1	0.2	0.3
V [m/s]	2 278	2 150	1 859
V_{Ag} [m/s]	2 096		
W_h [mm]	36	37	40
$W_{h,Ag}$ [mm]	37.7		
D_h [mm]	20	20	18

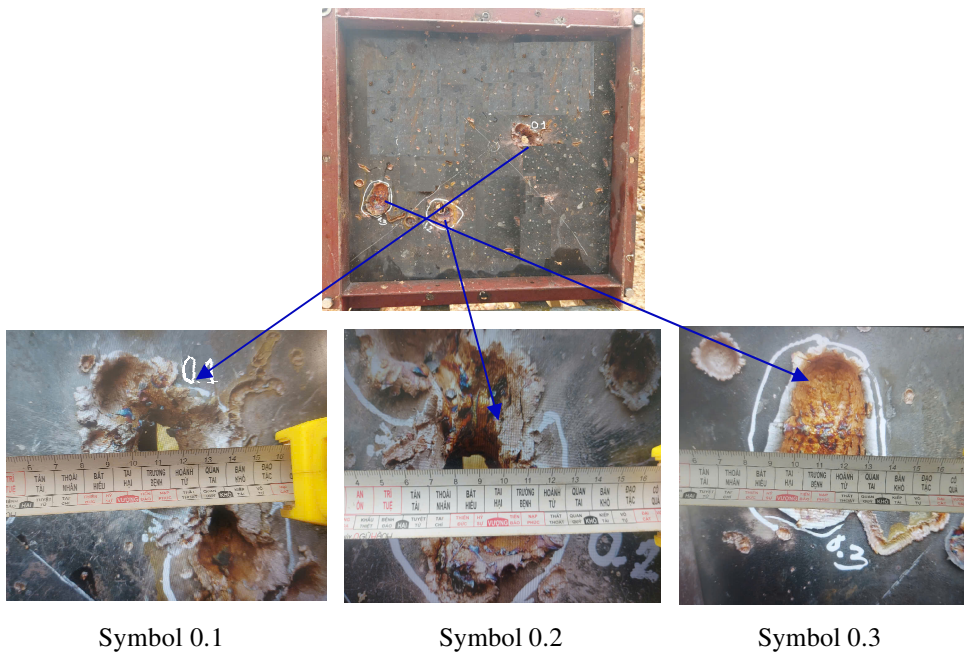


Fig. 5 Experimental results

4 Results and Discussion

Tab. 7 presents the results of the investigation on the impact of liner height on EFP formation in EFPW at time $t = 0.8$ ms for all EFPW structures with the parameters listed in Tab. 1.

4.1. Shape of EFP

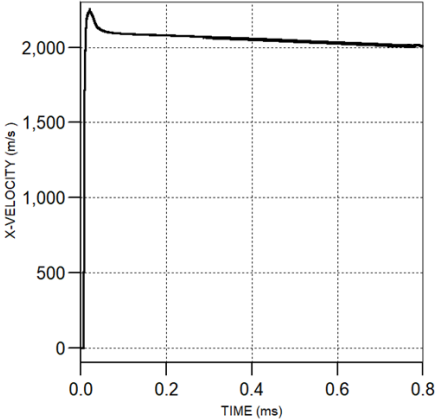
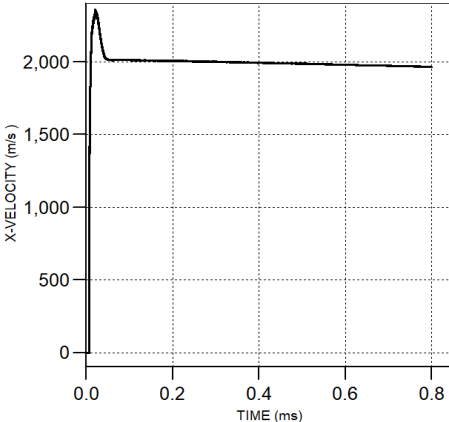
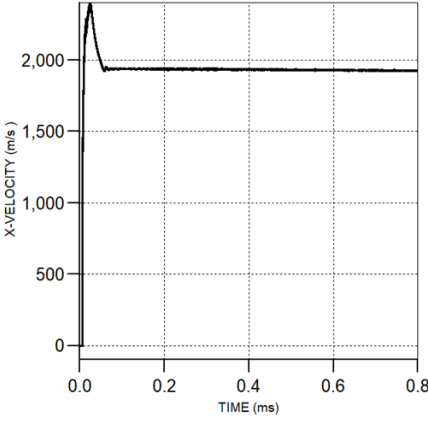
According to the simulation results, five EFPs with different shapes were formed under the action of the detonation wave on the liner after the explosive was detonated. The EFP formation processes at specific times and displacements are illustrated in Tab. 7.

When the ratio $h/d \leq 0.15$ as in structure 1, the EFP has a large diameter, resulting in poor aerodynamic shape. This causes significant energy loss during flight, reducing its penetration depth into the target.

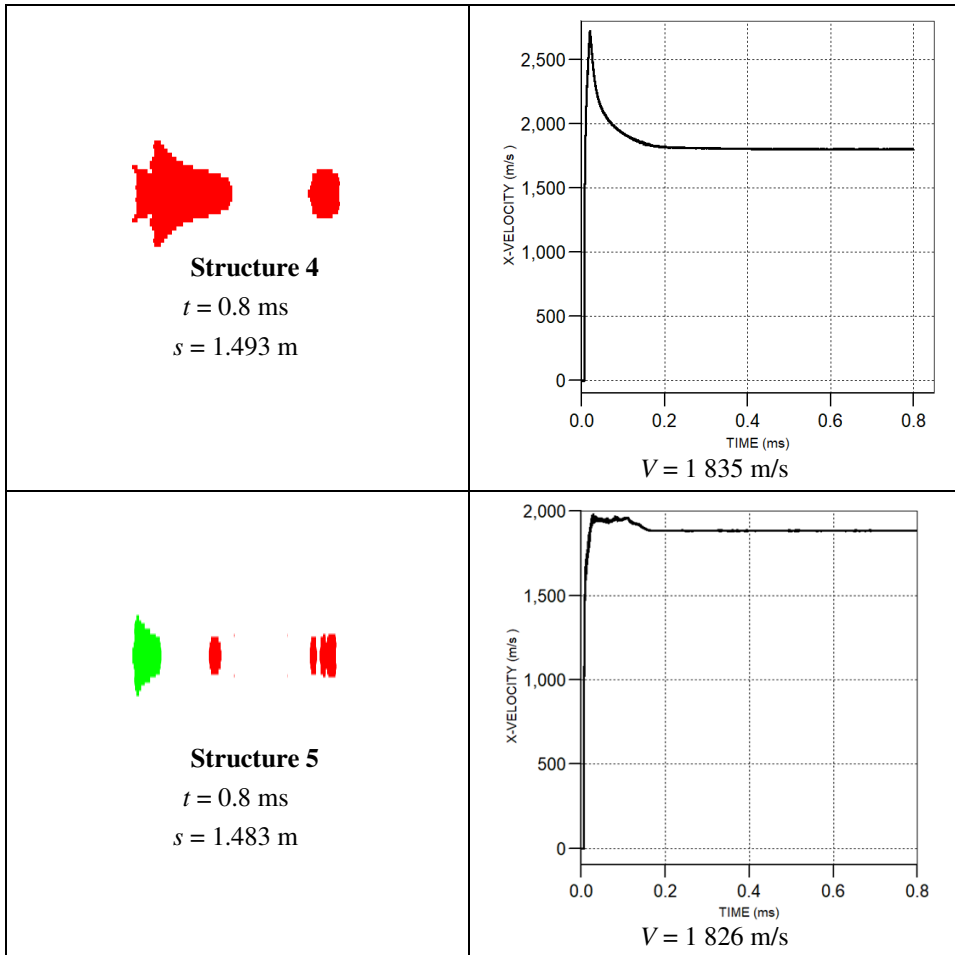
For configurations where h/d is within $(0.2 \div 0.3)$, structures 2 and 3 correspond, and the EFP has a streamlined, aerodynamically efficient shape. This allows it to travel longer distances and penetrate deeper into the target.

However, with $0.3 \leq h/d \leq 0.35$ as in structures 4 and 5, the EFP tends to elongate and fragment into smaller pieces. This reduces its penetration depth upon impact on the target.

Tab. 7a Shape and dynamic parameters of EFP

 <p>Structure 1 $t = 0.8 \text{ ms}$ $s = 1.655 \text{ m}$</p>	 <p>$V = 1\,992 \text{ m/s}$</p>
 <p>Structure 2 $t = 0.8 \text{ ms}$ $s = 1.638 \text{ m}$</p>	 <p>$V = 1\,957 \text{ m/s}$</p>
 <p>Structure 3 $t = 0.8 \text{ ms}$ $s = 1.594 \text{ m}$</p>	 <p>$V = 1\,927 \text{ m/s}$</p>

Tab. 7b Shape and dynamic parameters of EFP



4.2. Velocity of EFP

EFP velocity is one of the most important factors that greatly affects the ability to penetrate the target. The simulation and experimental results when EFP is formed with liner height are shown in Fig. 6.

For structures with a small shaping liner height $h/d \leq 0.15$, due to poor aerodynamic shape, the achieved velocity is the lowest among the surveyed structures, at 1 992 m/s.

When the liner height is increased from 0.2 to 0.3 of the liner diameters, the velocity tends to increase. The highest velocity achieved is 1 957 m/s with structure 2, which also exhibits the longest displacement distance among the surveyed structures, measuring 1.638 m. Structure 3 achieves a velocity of 1 927 m/s and a displacement distance of 1.594 m.

For structures with large liner heights $0.3 \leq h/d \leq 0.35$, the phenomenon of EFP disintegration occurs, with a significant velocity difference among the elements of the

EFP. At the EFP top, the velocity can exceed 2 600 m/s, while at the EFP tail, the velocity drops to approximately 1 000 m/s.

Based on the results obtained from the experiment on structure 2, the velocities of the three test samples were 2 278 m/s, 2 150 m/s, and 1 859 m/s, respectively. The average EFP velocity of the three samples was 2 096 m/s, with a 6.6 % deviation compared to the simulation results. The difference between the simulation and experimental results was less than 15 %, which is within the allowable range.

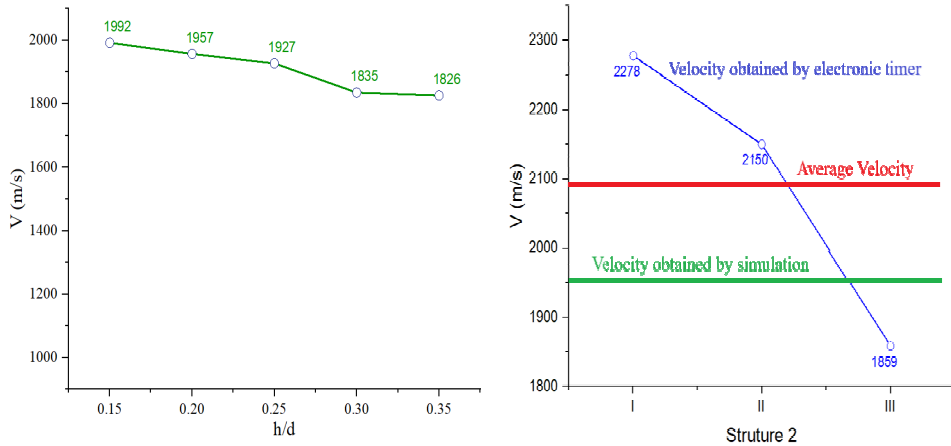


Fig. 6 Velocity of EFP obtained by simulation and experiments

4.3. Penetration Process

After forming, EFP begins to impact on 45# steel target plate. The thickness of the target plate is 30 mm. From Fig. 7, it can be seen that the material of the target plate was compressed under compressive and shear stresses, which are the main failure modes of the target when interacting with EFP. A combined tensile-compressive zone was observed in the front and rear of the steel plate. With the increasing penetration depth, the tensile zone began to dominate, which was caused by the significant elongation of the material at the edge of the shear zone. The reflection of the transverse wave at the rear surface and the penetration of EFP further aggravated the development of the damaged target. That is to say, there are two obvious active zones during the EFP penetration process, one is the compressive zone near the front surface of the target plate, where the target plate is mainly compressed, the other is the tensile zone near the back surface of the target plate, and the target plate in this zone is mainly tensile. As the penetration depth increases, the penetration of EFP is hindered and the damage zone becomes larger and larger.

The progression of damaged areas in the target plate for the five structures is shown in Fig. 8, based on the penetration diameter at the front and back surfaces of the steel plate. For structures 4 and 5, where the EFP is fragmented, the largest segment in terms of length and diameter is selected for simulating interaction with the steel plate. The simulation and experimental results when EFP penetrates the steel plate for hole diameters and penetration depths with different liner heights are shown in Fig. 9.

The penetration diameter at the front of the plate in structure 2 is the largest, and the diameter is 36 mm. The diameters in structures 1, 3, 4 and 5 are 34 mm, 26 mm,

24 mm, and 23 mm, respectively. In structures 1, 2 and 5, the rear-surface diameter of the penetration hole tends to be smaller than the front-surface diameter. Meanwhile, for structures 3, and 4, the diameters of the penetration holes on the front and rear surfaces are relatively uniform. This is attributed to the shape of the EFP when it impacts the steel plate.

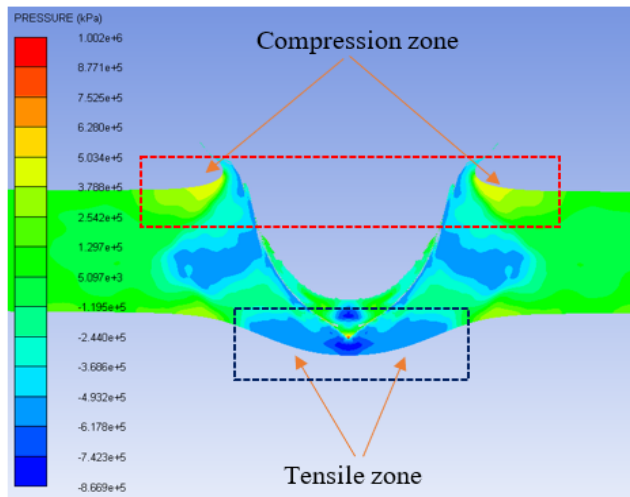


Fig. 7 EFP load bearing steel plate

From the experimental results on structure 2, the penetration diameters of the three test samples were 36 mm, 37 mm, and 40 mm, respectively, with an average penetration diameter of 37.7 mm. The discrepancy between the simulation and experimental results was less than 4.5 %, well within the acceptable margin of error.

The EFP achieves a maximum penetration depth of 25 mm when interacting with the steel plate, corresponding to structure 3. Structure 2 follows with a penetration depth of 23 mm. In contrast, the fragmented segments of structures 4 and 5 achieve depths of 19 mm and 17 mm, respectively. Structure 1 shows a minimal penetration depth of just 13 mm.

The experimental results indicate that two out of three test samples of structure 2 successfully pierced through the 20 mm thick steel target, while the remaining sample reached a penetration depth of 18 mm.

From the results of the survey on the formation and steel penetration of the EFP, it can be observed that for the studied EFPW model, there exists a height range of 0.2 to 0.3 times the liner diameter that allows achieving an optimal EFP shape. This greatly affects the warhead design, meeting combat requirements.

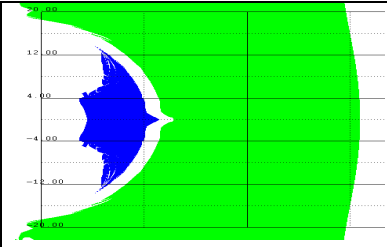
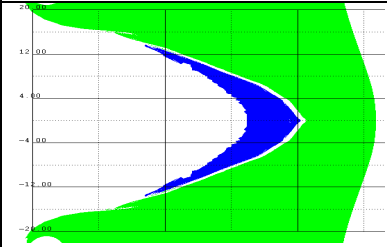
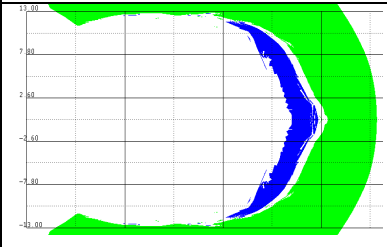
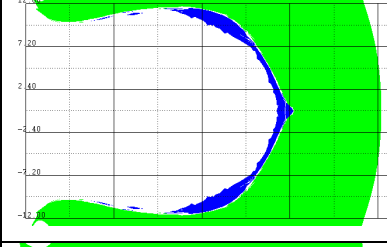
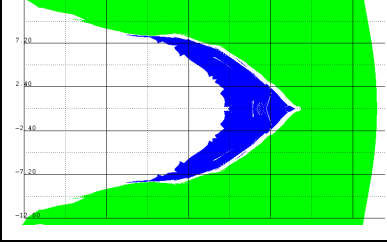
Structure 1		hole diameter $d_h = 34$ mm; hole length $b = 13$ mm
Structure 2		hole diameter $d_h = 36$ mm; hole length $b = 23$ mm
Structure 3		hole diameter $d_h = 26$ mm; hole length $b = 25$ mm
Structure 4		hole diameter $d_h = 24$ mm; hole length $b = 19$ mm
Structure 5		hole diameter $d_h = 23$ mm; hole length $b = 17$ mm

Fig. 8 EFP penetration process for different liner height

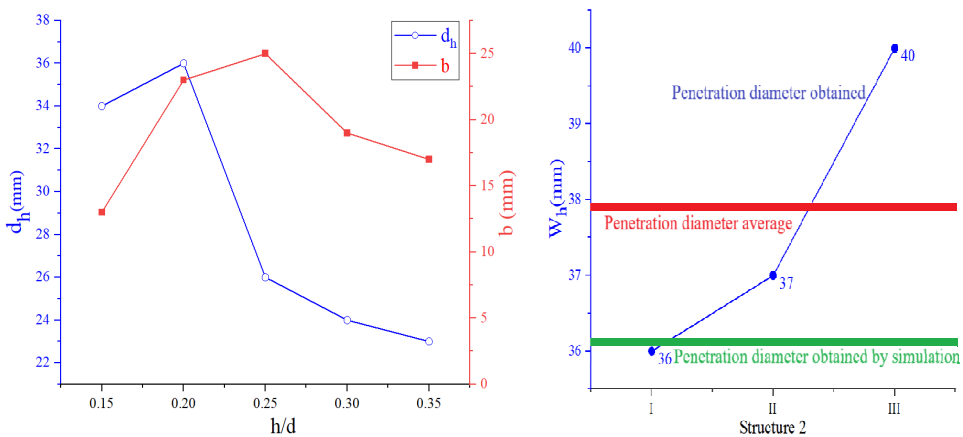


Fig. 9 Diameter and depth of EFP obtained by simulation and experiments

5 Conclusions

A finite element (FE) model was developed using Eulerian and Lagrangian methods to investigate the impact of liner height on the formation and penetration behavior of EFPs. Through the proposed FE model, the entire process of EFP formation and penetration, under varying liner heights, was thoroughly analyzed. The key findings are summarized as follows:

- The height of the liner has a direct influence on the dynamic characteristics, shape of the EFP, and its penetration performance against steel target plates. An optimal liner height, ranging from 0.2 to 0.3 times the liner diameter, ensures that the EFP achieves the best possible dynamic parameters and shape during formation.
- The minimum error between the numerical simulation method and the experiment of EFP velocity is less than 6.6 %, the simulated through hole diameter compared with the minimum error obtained is less than 4.5 % from the experimental method. It has been demonstrated that the proposed EFP model has high accuracy.
- The failure of the target material primarily occurs due to compressive and shear stresses. Additionally, the reflection of transverse waves at the rear surface and the EFP's penetration exacerbate the progression of material damage.

The optimization of EFPW design is a crucial challenge. This research provides valuable guidance for designers to achieve higher velocities and greater penetration depths by effectively integrating various geometric parameters.

References

- [1] ANDREEV, S.G., et al. *Physics of Explosion* (in Russian). 3rd ed. Moscow: Fizmatlit, 2004. ISBN 978-5-9221-0218-6.
- [2] ORLENKO, L.P. *Physics of Explosion and Impact* (in Russian). 2nd ed. Moscow: Fizmatlit, 2008. ISBN 978-5-9221-0891-1.

-
- [3] CARDOSO, D. and F. TEIXEIRA-DIAS. Modelling the Formation of Explosively Formed Projectiles (EFP). *International Journal of Impact Engineering*, 2016, **93**, pp. 116-127. DOI 10.1016/j.ijimpeng.2016.02.014.
- [4] WU, J., J. LIU and Y. DU. Experimental and Numerical Study on the Flight and Penetration Properties of Explosively Formed Projectile. *International Journal of Impact Engineering*, 2007, **34**(7), pp. 1147-1162. DOI 10.1016/j.ijimpeng.2006.06.007.
- [5] SALKIČEVIĆ, M. Numerical Simulations of the Formation Behavior of Explosively Formed Projectiles. *Defense and Security Studies*, 2022, **3**, pp. 1-14. DOI 10.37868/dss.v3.id183.
- [6] JEREMIĆ, O., M. MILINOVIĆ, M. MARKOVIĆ and B. RAŠUO. Analytical and Numerical Method of Velocity Fields for the Explosively Formed Projectiles. *FME Transactions*, 2017, **45**, pp. 38-44. DOI 10.5937/fmet1701038J.
- [7] COUQUE, H. and R. BOULANGER. EFP Simulations with Johnson-Cook Models. In: *23rd International Symposium on Ballistics*. Tarragona: ISB, 2007, pp. 255-262.
- [8] COUQUE, H., R. BOULANGER and F. BORNET. A Modified Johnson-Cook Model for Strain Rates Ranging from 10^3 to 10^5 s⁻¹. *Journal de Physique IV (Proceedings)*, 2006, **134**, pp. 87-93. DOI 10.1051/jp4:2006134015.
- [9] HUSSAIN, G., A. HAMEED, J.G. HETHERINGTON, P.C. BARTON and A.Q. MALIK. Hydrocode Simulation with Modified Johnson-Cook Model and Experimental Analysis of Explosively Formed Projectiles. *Journal of Energetic Materials*, 2013, **31**(2), pp. 143-155. DOI 10.1080/07370652.2011.606453.
- [10] LI, B.Y., et al. Orthogonal Optimization Design and Experiments on Explosively Formed Projectiles with Fins. *International Journal of Impact Engineering*, 2023, **173**, 104462. DOI 10.1016/j.ijimpeng.2022.104462.
- [11] LEE, E., M. FINGER and W. COLLINS. *JWL Equation of State Coefficients for High Explosives* [online]. 1973 [viewed 2025-10-12]. DOI 10.2172/4479737. Available from: <https://www.osti.gov/servlets/purl/4479737>.
- [12] JOHNSON, G.R. and W.H. COOK. Fracture Characteristics of Three Metals Subjected to Various Strains, Strain Rates, Temperatures and Pressures. *Engineering Fracture Mechanics*, 1985, **21**(1), pp. 31-48. DOI 10.1016/0013-7944(85)90052-9.
- [13] *ANSYS Autodyn User's Manual* [online]. 2018 [viewed 2025-10-20]. Available from: <https://www.scribd.com/document/453341462/ANSYS-Autodyn-Users-Manual-pdf>
- [14] VAZIRI, M.R., M. SALIMI and M. MASHAYEKHI. A New Calibration Method for Ductile Fracture Models as Chip Separation Criteria in Machining. *Simulation Modelling Practice and Theory*, 2010, **18**(9), pp. 1286-1296. DOI 10.1016/j.simpat.2010.05.003.